International Journal of Minerals, Metallurgy and Materials
Volume 27, Number 8, August 2020, Page 1147
https://doi.org/10.1007/s12613-020-2071-7

Reusing oxide-based pulverised fly ash and medical waste particles to develop electroless nickel composite coatings (Ni–P/fly ash and Ni–P/SiO_2–Al_2O_3)

Franco Mayanglambam[1,2] *and Mark Russell*[1)]

1) School of Natural and Built Environment, Queen's University Belfast, Belfast BT7 1NN, UK
2) Centre for Nanotechnology, Indian Institute of Technology Guwahati, Guwahati 781038, India
(Received: 5 January 2020; revised: 3 April 2020; accepted: 15 April 2020)

Abstract: Recycling and reusing materials from waste have become a nexus in the development of sustainable materials, leading to more balanced technologies. In this study, we developed a composite coating by co-depositing recycled ceramic particles, pulverised fly ash (PFA) and medical ceramics (MC), into a nickel–phosphorus matrix using a typical electroless plating process. Scanning electron microscopy (SEM) images indicated well-dispersed particles in the Ni–P matrix. However, compared with the MC particles, the PFA particles were distributed scantily with a lower content in the matrix, which could be due to the less impingement effect during the co-deposition. A modified microstructure with refined grains was obtained for the PFA-incorporated composite coating, as seen in the SEM micrograph. The X-ray diffraction result of the MC-incorporated composite coating showed the formation of Ni_xSi_y phases in addition to the typical Ni_3P phases for the heat-treated electroless Ni–P coatings. Upon heat treatment, the PFA-reinforced composite coating, due to a modified microstructure, exhibited a higher microhardness up to $HK_{0.05}$ 818, which is comparable to that of the traditional SiC particle-embedded composite coating ($HK_{0.05}$ 825). The findings can potentially open up a new strategy to further advance the green approach for industrial surface engineering.

Keywords: electroless plating; waste ceramics; fly ash particles; microstructure; microhardness

1. Introduction

In recent years, there has been a surge in the reinforcement of materials to suit a wide range of engineering applications. Various types of ceramics as reinforcing particles have been studied to manufacture Ni–P/X composite coatings by the versatile and cost-effective electroless nickel plating, where X represents Al_2O_3, SiO_2, TiO_2, SiC, etc. Oxide and carbide ceramic powders are increasingly used to reinforce metal matrixes to develop hard surfaces [1–7]. However, other relatively costly techniques are available to develop ceramic-based coatings, such as thermal spraying, physical vapor deposition (including magnetron sputtering, vacuum evaporation, and pulsed laser deposition), chemical vapor deposition, and molecular beam epitaxy.

The early works on the development of composite coating based on electroless nickel can be dated back to 1966 [8–10], in which Al_2O_3 was used as reinforcing particles. Electroless coatings incorporated with Al_2O_3 and SiO_2 particles have been used for diverse engineering applications concerning mechanical properties and corrosion resistance [3–6,11–14]. In addition, silicon-incorporated composite materials have also been used in semiconductor devices in which nickel silicide phases play a key role in adhesion and electrical properties [15–17]. Apachitei *et al*. [18] and Dong *et al*. [4] respectively investigated Ni–P/Al_2O_3 and Ni–P/SiO_2 composites and detailed the enhancement of micromechanical property with homogeneous particles dispersion. Recently, Ardakani *et al*. [5] reported the incorporation of nano-SiO_2 and nano-Al_2O_3 particles to develop Ni–P/SiO_2/Al_2O_3 composite and correlated its microhardness with its corrosion resistance behavior. However, the literature on the use of oxide ceramics from waste sources to develop composite coatings is limited. The few available reports include the study of a recycled particle-based composite coating such as Ni–P/fly ash [19] and the utilization of waste seashell-based ceramics [20] to develop Ni–P/seashell biocomposite coatings considering adhesion and anti-wear properties.

In this work, oxide-based waste ceramic particles (pulverised fly ash and medical waste) are reused to economically develop a composite coating (Ni–P/fly ash and Ni–P/SiO_2–Al_2O_3) using electroless nickel plating process.

Corresponding author: Franco Mayanglambam E-mail: fmayanglambam01@qub.ac.uk

Since the chemical composition of the waste ceramics is based on silicon and aluminum, the particles were rationally chosen, so that they could exhibit behaviors similar to that of the traditional hard silicon- and aluminum-based ceramic particles such as SiC, SiO_2, and Al_2O_3. In the present investigation, SiC particles were used for comparative purposes in terms of their incorporation in the nickel matrix, thickness build-up, and the resulting microhardness. The microstructure, particle settlement, distribution, chemical composition, and phase structure were analyzed using an optical microscope, a scanning electron microscope equipped with an energy-dispersive X-ray spectrometer, and an X-ray diffractometer. The resulting microhardness of the coating was also studied using a micro-indenter.

2. Experimental

Waste ceramics from medical device manufacturers (medical ceramics, MC) and thermal power plants (pulverised fly ash, PFA) consisting mainly of oxides of aluminum and silicon (Al_2O_3 and SiO_2) were used as reinforcing particles to develop composite coatings. The MC waste (whitish) was from an orthopedic implant mass finishing process, while the PFA ceramics waste (grayish) was supplied by Power Minerals Ltd., Drax Power Station, UK. The chemical compositions of the waste ceramics obtained from X-ray Fluorescence (XRF) analysis are given in Table 1. Both waste ceramics had similar chemical compounds and nearly the same weight percentages of SiO_2; however, the PFA had lower Al_2O_3 content. Aluminum alloy, LM24, with dimensions of 50 mm × 50 mm × 2 mm was used as a substrate. The chemical composition of the substrate is given in Table 2. Before the ceramic particles were introduced into the plating bath, they were sieved down using a 45 μm sieve. The particles were used as-received in dry powder without further treatment. Prior to the plating process, the particles were stirred for about 30 min in a medium-phosphorus electroless nickel bath (NiKlad ELV 808MX, MacDermid). A schematic representation of the plating process setup is shown in Fig. 1. The process conditions and parameters of the substrate surface pre-treatment and preparation of the electroless nickel composite coating are presented in Tables 3 and 4, respectively. For the pre-treatment, all the chemicals were R&D grade from Aldrich Ltd., UK. Based on the authors' earlier work [21] in which SiC microparticles were used, in the current study, the low (2 $g \cdot L^{-1}$) and high (18 $g \cdot L^{-1}$) concentration of the waste ceramic particles (SiC, MC, and PFA) in the plating bath were used, respectively. Furthermore, for comparison of the influence of the geometrical shape of the ceramic particles on the coating content, 2 $g \cdot L^{-1}$ ceramics (SiC and PFA, 1:1) comprising 1 $g \cdot L^{-1}$ angular SiC (particle sizes of 2–7 μm) and 1 $g \cdot L^{-1}$ round PFA were used in the plating solution. However, such a geometrical shape study was not conducted for the higher concentration of 18 $g \cdot L^{-1}$. The particle size of PFA was less than 45 μm (mesh size used to sieve down), and the average particle size was found to be 0.83 μm. The pH was increased using ammonium hydroxide (~50vol%) or decreased with H_2SO_4 (10vol%), based on the authors' earlier works [21–23].

Table 1. XRF data for compositions of the two ceramic particles wt%

Compound	MC	PFA
SiO_2	51.0	55.4
Al_2O_3	43.4	23.6
Fe_2O_3	0.5	4.8
TiO_2	0.9	1.0
MgO	0.2	1.8
CaO	0.2	4.7
K_2O	3.0	1.9

Table 2. Chemical composition of aluminum alloy (LM24) substrate wt%

Si	Cu	Mg	Zn	Fe	Mn	Ni	Pb	Sn	Ti	Al
8	3.5	3.0	3.0	1.3	0.5	0.5	0.3	0.2	0.2	Bal.

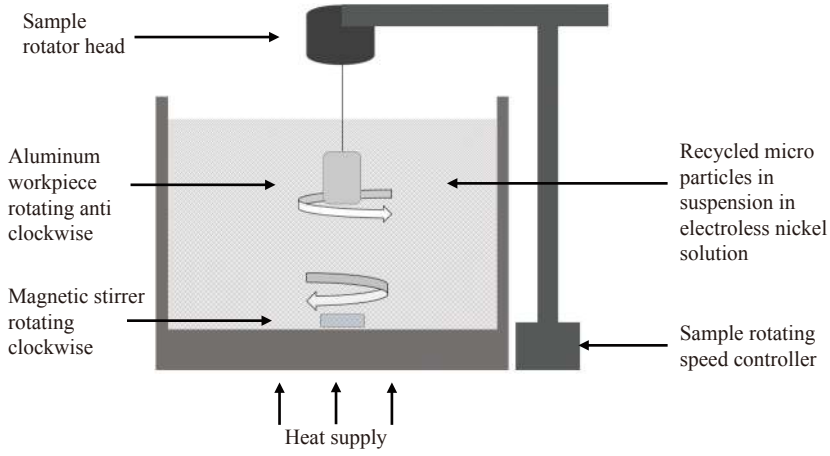

Fig. 1. Schematic representation of the setup for composite materials deposition process.

Table 3. Pre-treatment processes of aluminum substrate prior to plating

Process	Chemical	Temperature	Duration	Degree of agitation
Degreasing	C_6H_6O	Room temperature	3–5 min	None
Alkaline cleaning	5.75 g·L^{-1} Na_3PO_4 and 5.75 g·L^{-1} Na_2O_3Si	60–65°C	~3 min	Mild
Acid neutralizing	13vol% HNO_3	Room temperature	~20 s	Mild
Zincating	100 g·L^{-1} ZnO and 525 g·L^{-1} NaOH	Room temperature	~20 s	Mild

Table 4. Plating process condition

Ni metal concentration / (g·L^{-1})	5.4–6.3
$NaPO_2H_2$ concentration / (g·L^{-1})	27–33
Ceramics concentrations / (g·L^{-1})	2 and 18
pH value	4.8–4.9
Temperature / °C	88 ± 2
Duration / min	80
Agitation	Magnetic stirrer along with sample rotator

The coated samples were rinsed thoroughly with running water and air-dried. The samples were cut for different analyses, including microstructural and chemical analyses. The chemical composition was analyzed using field-emission scanning electron microscopy (FESEM, QUANTA FEG250) coupled with energy-dispersive X-ray spectroscopy (EDX, OXFORD X-Act); the phase structure was investigated using X-ray diffraction (XRD, PANalytical X-ray diffractometer) with CuK_α radiation of 0.154 nm wavelength; the microhardness was studied by the microindentation technique (Leco M-400). Heat treatment was isothermally performed in a furnace at 400°C for 1 h. For cross section study, the samples were mounted for metallographic analysis, which involved hot pressing, grinding, and polishing. Microindentation test was conducted on polished cross sections using a Knoop indenter under a load of 0.49 N; the measurement was conducted on at least five locations, and the average was recorded.

3. Results and discussion

3.1. Microstructure analysis

The XRD patterns for PFA and MC particles are shown in Fig. 2. The crystalline peaks consist of quartz and mullite phases, indicating the presence of silica and alumina compounds, which agrees with the XRF data in Table 1. A strong-intensity peak at $2\theta = 26°–27°$ is the typical diffraction pattern from quartz (precisely at 26.53°). Identical peaks were observed for both PFA and MC particles. Particle settlement in the metal matrix is clear from the micrographs (Fig. 3). A small amount of about 4vol% particles was observed in the coating prepared using 2 g·L^{-1} ceramic particles. The higher concentration of 18 g·L^{-1} ceramic particles yielded about 10vol% particles in the coating. The volumetric percentage was calculated from an image analysis software for comparative purposes. The traditional dissolution method was not adopted. The particle co-deposition in the nickel metal matrix occurred simply by the impingement of the former into the latter [8]. The particles become enveloped in the matrix as the thickness builds up. During the composite coating process using these waste ceramics, a surfactant was not added. In the absence of a surfactant, the even distribution of the particles in the coating was due to the random liquid flow during the process. The liquid flow, which was created by a magnetic stirrer at the bottom, was made non-unidirectional with the sample rotation by using a rotator that rotated the sample against the liquid flow, as represented in the schematic diagram of Fig. 1. The liquid flow is an important factor affecting the composite plating as it would determine the degree of distribution and particle stability while the particles are suspended in the bath. Preliminary trials have proved that the incorporation of the particles is better compared with using air agitation or the magnetic stirrer alone.

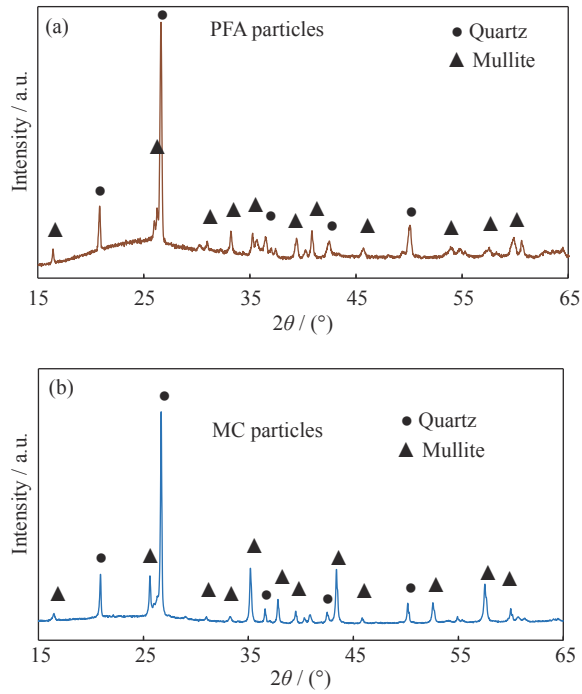

Fig. 2. XRD patterns for (a) PFA and (b) MC particles exhibiting similar peaks.

For the MC-embedded composite coating, the smaller particles settled at an early stage of the deposition process as

observed along and near the substrate–coating interface, whereas the larger particles were found at a later stage and deposited a slight distance away from the substrate, when the coating was already reasonably thick (Fig. 4). The coating thickness was smaller than expected, which could be due to the increase in the viscosity hindering the ionic mobility and eventually reducing the autocatalytic activity. The larger thickness obtained when the lower concentration of ceramic particles was used (Fig. 3) confirms a higher deposition rate owing to the lower viscosity. The thickness build-ups for different ceramic particles, with different concentrations in the plating solution, are compared later. An interesting observation is that the incorporation levels of the particles differed based on their geometrical shapes. The impingement of the irregular-shaped particles appeared to be better. The angular knife-like particles could have been held longer at the coating surface during the co-deposition process than the round particles. In the composite coating prepared using PFA particles, the spherical particles content was significantly low (Fig. 5(a)). The perfectly spherical PFA particles are susceptible to easily slip away during the co-deposition, reducing their possibility of being enveloped in the matrix. Hence, the impingement efficiency is reduced, resulting in the decrease of the embedded PFA particles content. The coating prepared using plating solution containing 1:1 proportion of differently shaped ceramic particles (Fig. 5(b)) further elucidates the difference in incorporation levels based on the ceramic particles shape. The higher content of angular particles in the coating than that of spherical particles confirms the efficiency of the former in settling in the matrix than the latter through impingement. The result is somewhat contradictory to other findings [18,24], which reported a better efficiency of spherical particles in incorporating into the coating. However, irregular-shaped particles are generally believed to be effectively held in the coating [8]. During metallographic sample preparation, the small spherical particles are not prone to dislodging once settled, in contrast with the angular particles, which generate abrasive lines from slight movements and the rolling of the dislodged particles.

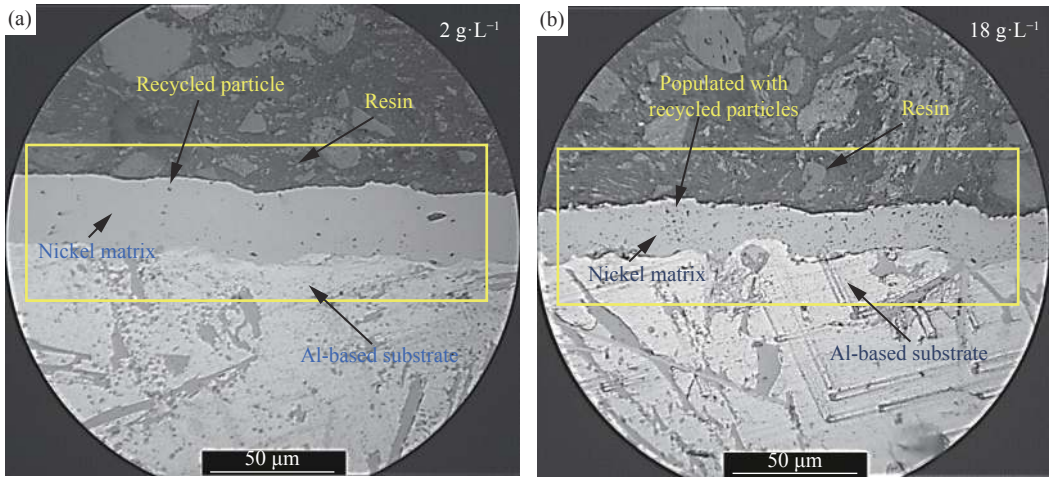

Fig. 3. Cross sections showing MC contents in the coatings for two different concentrations of ceramic particles in the plating solution: (a) 2 g·L^{-1}; (b) 18 g·L^{-1}.

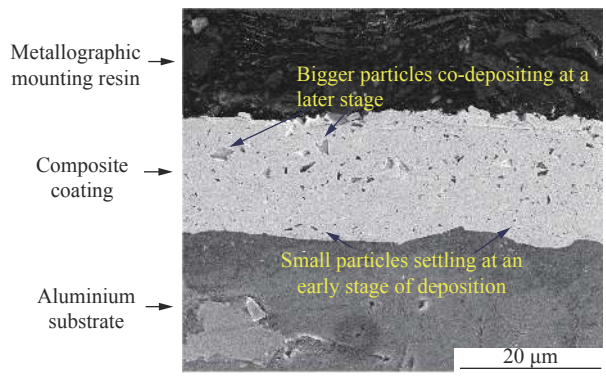

Fig. 4. MC particle size distribution in the coating (18 g·L^{-1} MC particles) showing the smaller and larger particles.

The viscosity of the MC-containing bath was slightly higher than that of the PFA-containing bath. As the present study focuses mainly on the changes in microstructure and the resulting microhardness of the coating, viscosity measurement and chemical composition variation in the bath are outside the scope of the work. The thickness build-ups for different ceramic particles are compared in Fig. 6. For the MC particles, a difference is seen between the coatings made from 18 and 2 g·L^{-1} particle concentrations: the coating obtained using a plating solution with higher MC concentration had lower thickness. On the contrary, using a solution with higher concentration of PFA particles did not affect the thickness build-up. The expected thickness was about 29 μm. No large difference in the deposition thickness was observed

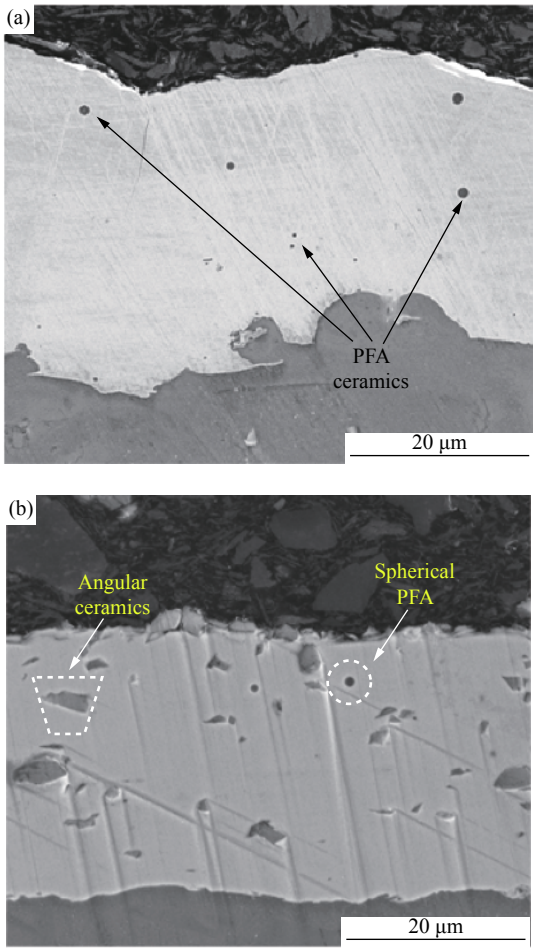

Fig. 5. Micrographs showing the incorporation and distributions of particles in the coatings from using (a) 2 g·L^{-1} PFA spherical ceramic particles and (b) angular and spherical ceramic particles in 1:1 (1 g·L^{-1} each of SiC and PFA particles).

between the coatings prepared with lower and higher concentrations of PFA particles. Thus, the results of the coating thickness, which is not largely influenced by the PFA particles, mean that the autocatalytic activity of the nickel solution is still preserved. In terms of stability or inertness, the PFA particles in the solution behave like the traditional SiC particles typically used in preparing Ni–P–SiC composites. Regarding the solution containing MC particles, the catalytic power is reduced by the possible soluble miscellaneous chemicals, which are hygroscopic, and this eventually reduces the coating thickness.

The electroless nickel composite coating embedded with MC particles (18 g·L^{-1}) exhibited a typical cauliflower morphology (Fig. 7(a)), whereas the PFA particle-embedded (18 g·L^{-1}) composite coating exhibited a different morphology with a smaller and subglobular microstructure on the typical cauliflower structure (Fig. 7(b)). The spherical globular shape of the sub-cauliflower cluster could be from the mechanical impact of the larger PFA ceramic balls that could not be incorporated into the coating during the deposition due to size incompatibility. The refined grain morphology can be explained with the mechanically assisted Ni–P plating model using glass balls [25–26]. During the plating process, the larger spherical particles could produce a local disturbance in the electrolyte at the surface of the workpiece (substrate) to create a concentration gradient, accompanied by the mechanical impact of the particles on the substrate. The pressure exerted on the coating by repeated striking and rolling at the microscale could result in perturbation during the grain growth. A polycrystalline structure has been reported for mechanically assisted electroless nickel coating owing to the reduction in activation energy for partial crystallization due to the continuous pressure from glass balls (diameters of 2–3 mm) [26]. Herein, the size and weight of the PFA particles may not be sufficiently large enough to cause partial crystallization of the coating. However, grain refinement was observed; it created internal stress, which is beneficial for improving mechanical

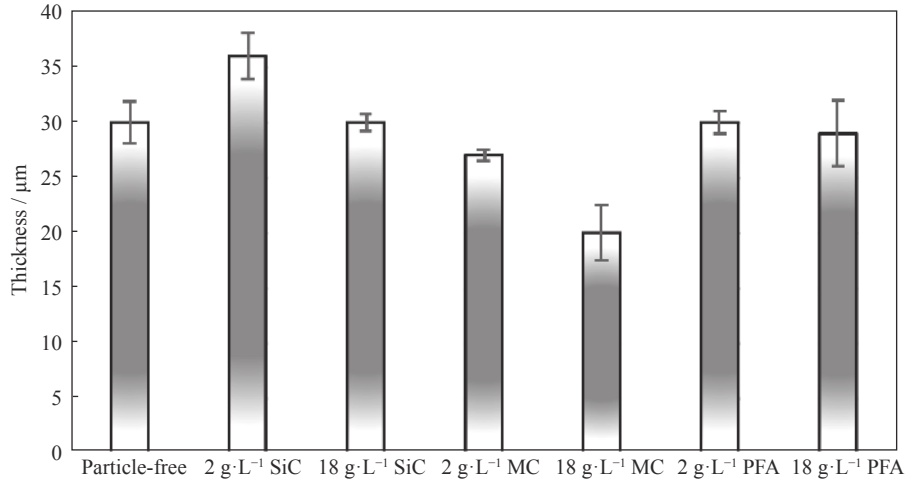

Fig. 6. Thickness build-ups from using particle-free plating solution and solutions containing different concentrations of the traditional SiC particles and the MC and PFA particles.

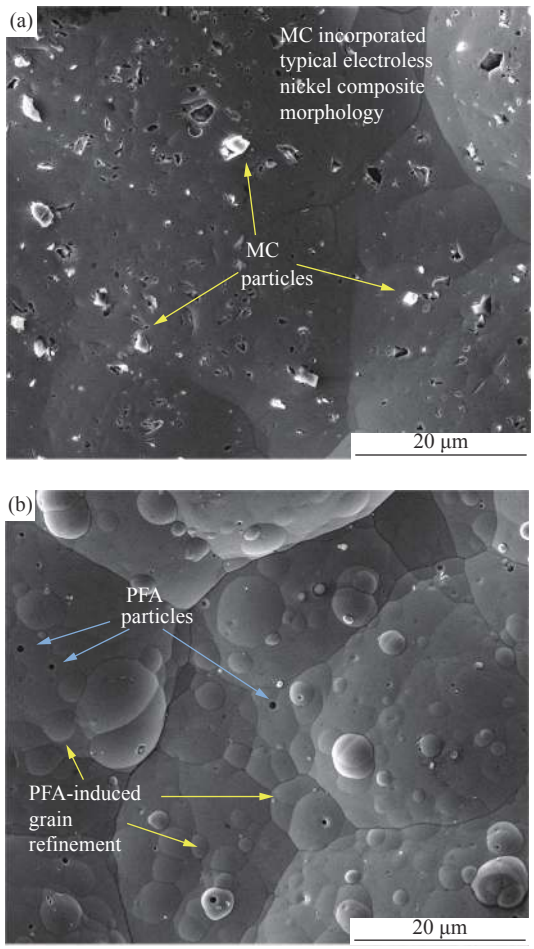

Fig. 7. Microstructures of Ni–P morphologies showing the effect of different ceramic particles (18 g·L^{-1}) incorporation: (a) MC; (b) PFA. Modified microstructure of refined grain is shown for coating with PFA particles.

properties. Another aspect of the evolution of the refined grains is the adsorption phenomenon of the foreign particles during the nucleation of the Ni–P. The PFA spherical particles are transported at the vicinity of the metal piece via convective diffusion and adsorbed at the active sites. During the grain growth, further growth of the Ni–P nodules is inhibited due to the interruption of the adsorbed particles, thereby reducing the grain size. As the particles are adsorbed on the catalytic sites, they could also act as nuclei for crystal growth [27]. Balaraju and Rajam [28] reported the activation of natural nucleation sites by the introduction of ions such as Cu, which retarded the nodule growth, resulting in the refined nodule size of the morphology. Hence, the grain refinement of the PFA-incorporated composite coating with a smaller globular microstructure is explained by the mechanically assisted plating model and adsorption phenomenon.

The EDX analysis results of the MC-incorporated (18 g·L^{-1}) composite coatings reveal the significant peaks that correspond to Si, Al, and O (Fig. 8), confirming the presence of SiO_2 and Al_2O_3. Quartz is confirmed from the particles, which present a strong peak of Si. The particles with peaks of Al are alumina and mullite, as shown in the point spectrum of the corresponding particle. The cross section maps of the MC-incorporated coating show the distribution of specific particles (Figs. 9(a) and 9(b)). Both the Al- and Si-based particles are seen to disperse evenly. Clusters of the same particles are not observed. For the PFA-incorporated composite coating, the point analysis of a single spherical PFA particle gives the chemical composition as mainly oxides of Si and Al, as shown in the EDX spectrum in Fig. 9(c).

The diffused, single, and broad peaks in the as-deposited states in Fig. 10 show the amorphous phases of the composite coatings. Those are the typical hump shape of the electroless nickel coating that occurs at $2\theta = 40°–50°$. The as-deposited state of the SiC composite coating shows weak peaks at 35.7° and 60.1°, corresponding to SiC particles (Fig. 10(a)). Moreover, MC and PFA composite coatings do not show any typical diffraction peaks of the ceramics (Figs. 10(b) and 10(c)). The percentage of the incorporated ceramic particles is low and could have been overshadowed by the diffused peak of the amorphous Ni–P, which is in accordance with the XRD pattern reported by Panagopoulos and Georgiou [19]. In the case of the PFA-incorporated coating in the as-deposited state (Fig. 10(c)), polycrystallinity is not seen despite the grain refinement by the mechanical assistance of the spherical particles, as compared with that in the reported diffraction patterns from the mechanically assisted coating using glass balls [25–26]. The amorphous phase could be due to the insufficient mass and size of the particles in the suspension;

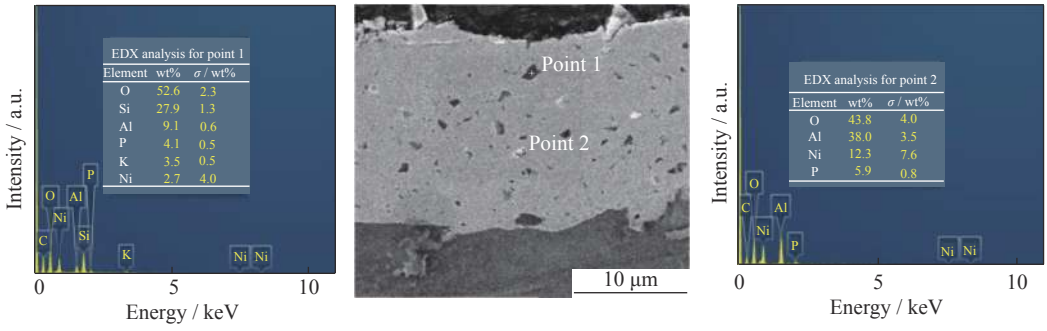

Fig. 8. Elemental analyses for specific particles in the Ni–P matrix for MC-incorporated (18 g·L^{-1}) coating (σ corresponds to error).

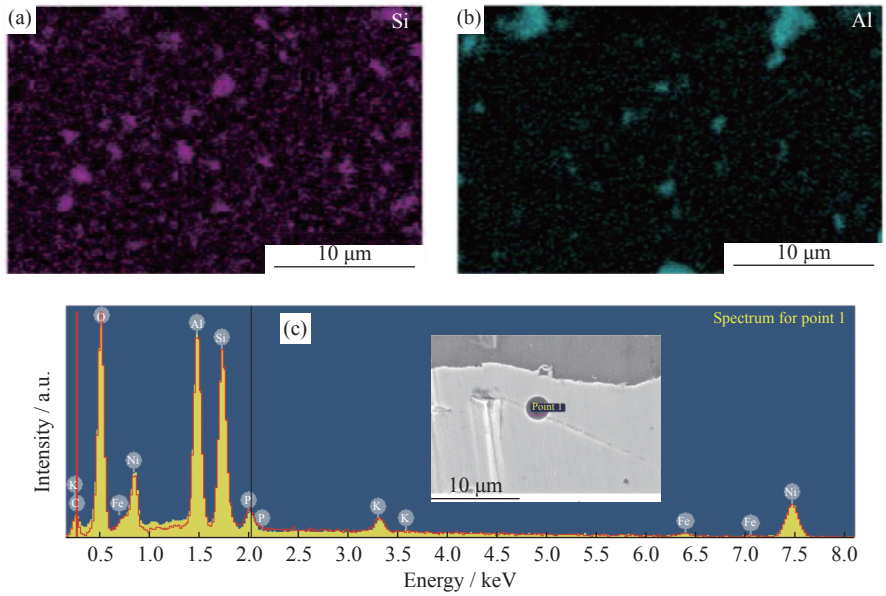

Fig. 9. EDX maps of the cross section showing the distribution of (a) Si and (b) Al due to SiO_2 and Al_2O_3 in the MC-incorporated (18 g·L^{-1}) composite coating; (c) EDX spectrum showing chemical composition of a spherical PFA particle in the PFA-incorporated composite coating.

comparatively, the impact of the particles on the substrate would have to be much lower to cause crystallinity. The amorphous state in a metal is metastable, and it can be transformed into a more stable crystalline state. The energy required for its transformation is generally provided by annealing. The phenomenon of crystallization by mechanically assisted plating is explained by classical thermodynamics. The mechanical pressure induced by the spherical balls reduces the energy barrier and hence facilitates the transformation from amorphous to the crystalline state. However, in the present study, the PFA spherical balls could not meet the impact requirement to reduce the energy barrier mechanically. Thus, the grain refinement of the PFA ceramic composite coating is assumed to be predominantly caused by the adsorption phenomenon, as discussed earlier.

Upon heat treatment, the evolution of the crystalline phases is mainly from Ni_3P and Ni for the SiC-, MC-, and PFA-embedded coatings. At 400°C, the formation (nucleation and growth) of Ni_3P phase occurs from the metastable phases in the untreated condition arising from the gradual segregation of phosphorus at the grain boundaries and triple junction. Consequently, the precipitation of Ni_3P phases occurs [28–31]. Additional peaks at about 47° and 48° for SiC- and MC-embedded coatings, respectively, are nickel silicide phases (Figs. 10(a) and 10(b)). Such peaks are absent in the PFA-incorporated composite coating owing to either the low content of Si from SiO_2 particles or the higher tendency of the local nickel content to react with P to form Ni_3P phase instead of reacting with Si to form Ni_xSi_y. For composites with SiC and MC particles, the Si contents in the coatings were higher and could be the right amount to initiate the bonding with Ni. Gao *et al*. [32] also reported that the formation of nickel silicides is driven by the available nickel content and the right amount of Si. The thermodynamically metastable clusters of nickel atoms diffuse and break into Si–*Y* bond (*Y* represents O in the present case) and initiate new bond formation. Only when the right amount of Si is consumed does the formation of nickel silicides (Ni_5Si_2) occur, and Ni_5Si_2 is subsequently transformed to Ni_3Si phases, as well as other phases [33–34]. Strong competition could exist between the available local phosphorus and silicon to form phases with nickel as phosphides and silicides, respectively [33–34]. Apachitei *et al*. [1] reported that under annealing at above 400°C, the partial decomposition of Si–C occurred. At a certain Si/C ratio, with increasing temperature, there becomes enough energy to break the Si–C bond. Thus, the nickel silicides evolution at around 47° and 48° could be any metastable phases arising from the diffusion of Ni into SiC and SiO_2.

3.2. Microhardness

The average microhardness results of MC- and PFA-incorporated (2 g·L^{-1}) coatings are shown in Fig. 11. Traditional nickel-based SiC particle-reinforced (2 g·L^{-1}) coatings are included for comparative purpose. The coatings incorporated with PFA particles showed improvement in microhardness. The increased hardness agrees with previously reported results [19] and is due to the presence of oxides such as SiO_2 and Al_2O_3 contained in fly ash in the Ni–P matrix of the coating. The average hardness for the as-deposited particle-free and SiC-, MC-, and PFA-incorporated coatings are $HK_{0.05}$ 411, 504, 443, and 505, respectively. In the as-deposited state, the

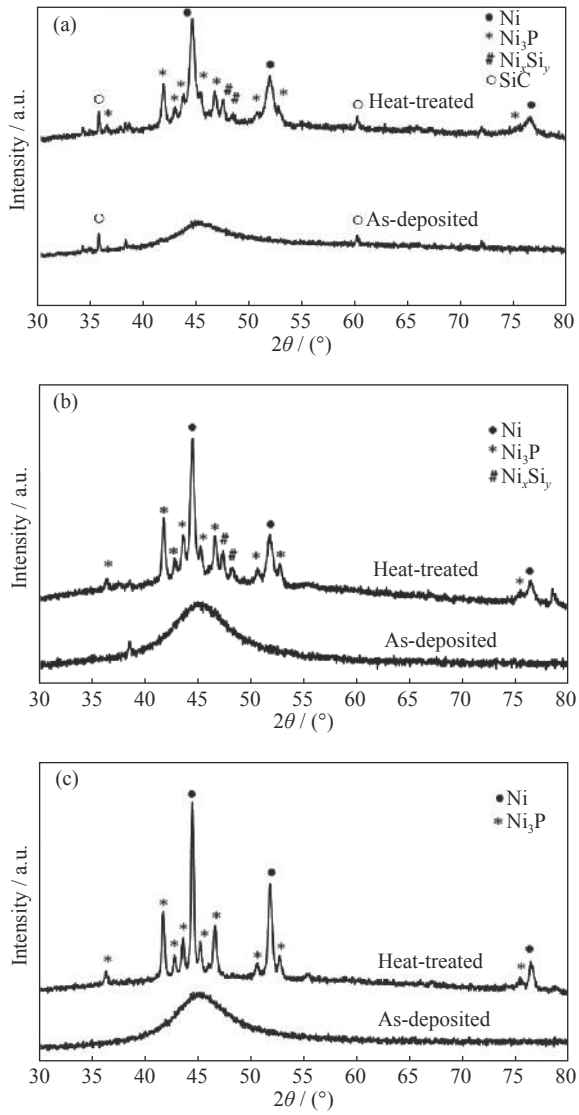

Fig. 10. XRD patterns for the as-deposited and heat-treated ceramic particle-incorporated (18 g·L^{-1}) composite coatings: (a) SiC, (b) MC, and (c) PFA.

higher microhardness of the PFA-reinforced coating, which is comparable to that of the SiC-reinforced coating, is due to grain refinement. Microstructure consisting of smaller grain sizes has more grain boundaries. It should be noted that in this paper when discussing amorphous coatings, "grains" refer to the nodular structure but not the crystallographic grains of crystalline materials. In general, when indenting on a crystalline material, the hardness is based on the permanent deformation arising from the dislocation slip. Grain boundaries act as obstacles to dislocation slip. With refined grains having more grain boundaries, the dislocation slip is interrupted due to random atom arrangement across the boundary, leading to higher hardness. Here, however, the Ni–P is amorphous but not crystalline, and thus, dislocations or a dislocation hardening theory is not applicable. The increase in microhardness could be governed by internal stress resulting from the grain refinement. Improved mechanical properties when Ni–P was incorporated with other waste ceramic particles to form Ni–P/biocomposite have also been reported by Jagatheeshwaran *et al*. [20].

Compared with the PFA-reinforced coating, the as-deposited state of the MC-reinforced coating did not show a large improvement in hardness despite having a higher content of embedded particles. The lack of significant increase in hardness can be analyzed from two aspects: microstructure and reinforcing particles. Grain size reduction from the effect of the particles was not observed. Impingement is predominant over particle adsorption on the coating, thus resulting in a high degree of incorporation. During grain growth, the angular and relatively smaller particles impinge on the Ni–P matrix. The particles are enveloped progressively at the surface without much effect of adsorption, preventing the creation of smaller vacant sites for the incoming nickel atoms to nucleate and produce refined grains. Hence, in the absence of a smaller globular microstructure, the microhardness of the MC coating was not improved compared with the PFA-embedded coating. Second, the original hardness of MC does not contribute much to the coating hardness.

Upon heat treatment, the average hardness is increased owing to the precipitation and crystallization hardening accompanied by the internal stress on the microstructure. The average microhardness in the heat-treated states for the particle-free and SiC-, MC-, and PFA-embedded coatings were $HK_{0.05}$ 638, 779, 537, and 729, respectively. The PFA composite coating exhibited higher hardness compared with the particle-free and MC-incorporated coatings. However, the microhardness of the PFA composite coating was comparable to that of the traditional SiC composite coating. In the PFA composite coating, the initial high hardness due to refined grain size in the as-deposited state could further enhance the hardness even after annealing. The increment in hardness for post-heat treatment is predominantly due to the microstructure of the matrix but not only from the ceramic particles present in the matrix. On the contrary, the heat-treated MC composite coating did not show large improvement despite the better degree of particle content in the matrix. The general increase in hardness upon annealing compared with the as-deposited state is due to the precipitation hardening with the formation of Ni_3P, as shown in the XRD patterns (Fig. 10). The maximum microhardness of $HK_{0.05}$ 818 was obtained for the PFA composite coating, which is comparable to the microhardness of $HK_{0.05}$ 825 for the traditional SiC composite coating.

The following research areas are suitable for future work:

(1) Elaborate analysis of the effects of using PFA particles with various sizes on the adsorption phenomena during the deposition at various intervals of the coating process.

(2) Higher-magnification transmission electron microscopy (TEM)-based investigation of the physicochemical be-

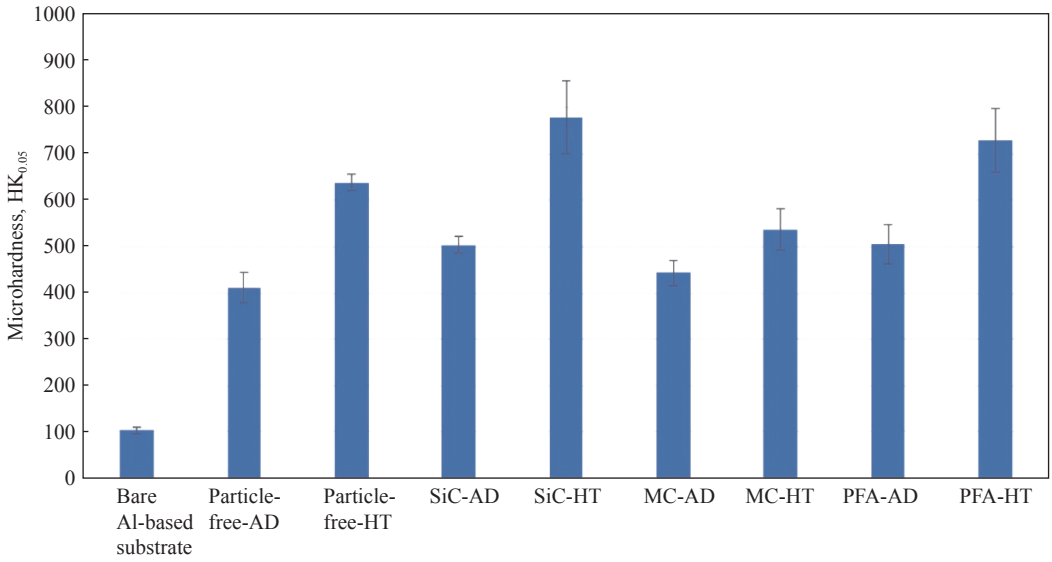

Fig. 11. Microhardness results of ceramic particles (SiC, MC, and PFA)-incorporated (2 g·L^{-1}) coatings and particle-free coatings. AD and HT refer to as-deposited and heat-treated states, respectively.

havior of the particle–matrix interface when subjected to a thermal environment.

(3) Investigation of the sliding tribological behavior of the waste ceramic-incorporated composite coating at room and elevated temperatures to study the variable parameters for surface engineering strategy in industrial scale.

4. Conclusions

In this study, waste ceramic particles (PFA and MC) were co-deposited into a nickel–phosphorus matrix using a typical electroless plating process to develop composite coatings. The research findings are outlined below:

(1) The waste ceramic particles (PFA and MC) were effectively incorporated into the Ni–P metallic matrix to develop a metal–ceramic matrix coating system as Ni–P/SiO_2–Al_2O_3-based waste particles.

(2) The composite coatings made from MC particles featured uniform dispersion of the particles in the matrix. The PFA particles, with a spherical shape, were distributed scantily with a lower content in the matrix, which could be due to less impingement effect. However, the PFA-embedded coating exhibited a modified microstructure with refined grain growth.

(3) The chemical analysis results suggest that the composite coatings featured scattered distribution of SiO_2 and Al_2O_3. Upon heat treatment, the coating with MC particles showed additional peaks of nickel silicides (Ni_xSi_y phases), arising from the relatively high content of the ceramic particles; this could be due to the diffusion of available nickel into SiO_2.

(4) The microhardness of the composite coating with PFA ceramic particles was improved. Upon heat treatment, the PFA-reinforced composite coating, due to a modified microstructure, exhibited higher microhardness up to $HK_{0.05}$ 818, comparable to that of the traditional SiC particle-embedded composite coating ($HK_{0.05}$ 825).

Acknowledgements

The continuous guidance by Prof. Wei Sha, the financial support from Queen's University Belfast, UK, in the form of a studentship, PFA powder provided by Ali Rafeet, and technical help from Jim Knox and his team from Queen's University Belfast, UK, are deeply appreciated. The suggestion from I. Neelakanta Reddy (Yeungnam University, Republic of Korea) is also appreciated.

References

[1] I. Apachitei, F.D. Tichelaar, J. Duszczyk, and L. Katgerman, Solid-state reactions in low-phosphorus autocatalytic NiP–SiC coatings, *Surf. Coat. Technol.*, 148(2001), No. 2-3, p. 284.

[2] P. Makkar, R.C. Agarwala, and V. Agarwala, Chemical synthesis of TiO_2 nanoparticles and their inclusion in Ni–P electroless coatings, *Ceram. Int.*, 39(2013), No. 8, p. 9003.

[3] N.K. Shrestha, D.B. Hamal, and T. Saji, Composite plating of Ni–P–Al_2O_3 in two steps and its anti-wear performance, *Surf. Coat. Technol.*, 183(2004), No. 2-3, p. 247.

[4] D. Dong, X.H. Chen, W.T. Xiao, G.B. Yang, and P.Y. Zhang, Preparation and properties of electroless Ni–P–SiO_2 composite coatings, *Appl. Surf. Sci.*, 255(2009), No. 15, p. 7051.

[5] S.R. Ardakani, A. Afshar, S. Sadreddini, and A.A. Ghanbari, Characterization of Ni–P–SiO_2–Al_2O_3 nano-composite coatings on aluminum substrate, *Mater. Chem. Phys.*, 189(2017), p. 207.

[6] Y. de Hazan, D. Zimmermann, M. Z'graggen, S. Roos, C. Aneziris, H. Bollier, P. Fehr, and T. Graule, Homogeneous electroless Ni–P/SiO_2 nanocomposite coatings with improved wear resistance and modified wear behaviour, *Surf. Coat. Technol.*,

204(2010), No. 21-22, p. 3464.
[7] S. Karthikeyan and B. Ramamoorthy, Effect of reducing agent and nano Al_2O_3 particles on the properties of electroless Ni–P coating, *Appl. Surf. Sci.*, 307(2014), p. 654.
[8] J.N. Balaraju, T.S.N. Sankara Narayanan, and S.K. Seshadri, Electroless Ni–P composite coatings, *J. Appl. Electrochem.*, 33(2003), No. 9, p. 807.
[9] J. Sudagar, J.S. Lian, and W. Sha, Electroless nickel, alloy, composite and nano coatings – A critical review, *J. Alloys Compd.*, 571(2013), p. 183.
[10] R.C. Agarwala and V. Agarwala, Electroless alloy/composite coatings: A review, *Sadhana*, 28(2003), p. 475.
[11] J.N. Balaraju, Kalavati, and K.S. Rajam, Influence of particle size on the microstructure, hardness and corrosion resistance of electroless N–P–Al_2O_3 composite coatings, *Surf. Coat. Technol.*, 200(2006), No. 12-13, p. 3933.
[12] S. Alirezaei, S.M. Monirvaghefi, M. Salehi, and A. Saatchi, Effect of alumina content on surface morphology and hardness of Ni–P–Al_2O_3(α) electroless composite coatings, *Surf. Coat. Technol.*, 184(2004), No. 2-3, p. 170.
[13] S. Alirezaei, S.M. Monirvaghefi, M. Salehi, and A. Saatchi, Wear behavior of Ni–P and Ni–P–Al_2O_3 electroless coatings, *Wear*, 262(2007), No. 7-8, p. 978.
[14] M. Novák, D. Vojtěch, and T. Vítů, Influence of heat treatment on tribological properties of electroless Ni–P and Ni–P–Al_2O_3 coatings on Al–Si casting alloy, *Appl. Surf. Sci.*, 256(2010), No. 9, p. 2956.
[15] A. Mondon, M.N. Jawaid, J. Bartsch, M. Glatthaar, and S.W. Glunz, Microstructure analysis of the interface situation and adhesion of thermally formed nickel silicide for plated nickel–copper contacts on silicon solar cells, *Sol. Energy Mater. Sol. Cells*, 117(2013), p. 209.
[16] C.M. Liu, W.L. Liu, S.H. Hsieh, T.K. Tsai, and W.J. Chen, Interfacial reactions of electroless nickel thin films on silicon, *Appl. Surf. Sci.*, 243(2005), No. 1-4, p. 259.
[17] A. Duhin, Y. Sverdlov, I. Torchinsky, Y. Feldman, and Y. Shacham-Diamand, NiSi contact metallization using electroless Ni deposition on Pd-activated self-assembled monolayer (SAM) on p-type Si(1 0 0), *Microelectron. Eng.*, 84(2007), No. 11, p. 2506.
[18] I. Apachitei, J. Duszczyk, L. Katgerman, and P.J.B. Overkamp, Electroless Ni–P composite coatings: The effect of heat treatment on the microhardness of substrate and coating, *Scripta Mater.*, 38(1998), No. 9, p. 1347.
[19] C.N. Panagopoulos and E.P. Georgiou, Surface mechanical behaviour of composite Ni–P–fly ash/zincate coated aluminium alloy, *Appl. Surf. Sci.*, 255(2009), No. 13-14, p. 6499.
[20] M.S. Jagatheeshwaran, A. Elayaperumal, and S. Arulvel, Impact of nano zinc oxide on the friction–wear property of electroless nickel–phosphorus sea shell composite coatings, *Mater. Sci. Eng. B*, 225(2017), p. 160.
[21] M. Franco, W. Sha, S. Malinov, and R. Rajendran, Phase composition, microstructure and microhardness of electroless nickel composite coating co-deposited with SiC on cast aluminium LM24 alloy substrate, *Surf. Coat. Technol.*, 235(2013), p. 755.
[22] M. Franco, W. Sha, S. Malinov, and H. Liu, Micro-scale wear characteristics of electroless Ni–P/SiC composite coating under two different sliding conditions, *Wear*, 317(2014), No. 1-2, p. 254.
[23] M. Franco, W. Sha, V. Tan, and S. Malinov, Insight of the interface of electroless Ni–P/SiC composite coating on aluminium alloy, LM24, *Mater. Des.*, 85(2015), p. 248.
[24] I. Apachitei, J. Duszczyk, L. Katgerman, and P.J.B. Overkamp, Particles co-deposition by electroless nickel, *Scripta Mater.*, 38(1998), No. 9, p. 1383.
[25] Z.X. Ping, Y.D. He, C.D. Gu, and T.Y. Zhang, Mechanically assisted electroplating of Ni–P coatings on carbon steel, *Surf. Coat. Technol.*, 202(2008), No. 24, p. 6023.
[26] Z.X. Ping, G.A. Cheng, and Y.D. He, Mechanically assisted electroless barrel-plating Ni–P coatings deposited on carbon steel, *J. Mater. Sci. Technol.*, 26(2010), No. 10, p. 945.
[27] X.W. Zhou, Y.F. Shen, H.M. Jin, and Y.Y. Zheng, Microstructure and depositional mechanism of Ni–P coatings with nano-ceria particles by pulse electrodeposition, *Trans. Nonferrous Met. Soc. China*, 22(2012), No. 8, p. 1981.
[28] J.N. Balaraju and K.S. Rajam, Electroless deposition of N–Cu–P, Ni–W–P and Ni–W–Cu–P alloys, *Surf. Coat. Technol.*, 195(2005), No. 2-3, p. 154.
[29] I. Apachitei, F.D. Tichelaar, J. Duszczyk, and L. Katgerman, The effect of heat treatment on the structure and abrasive wear resistance of autocatalytic NiP and NiP–SiC coatings, *Surf. Coat. Technol.*, 149(2002), No. 2-3, p. 263.
[30] T. Hentschel, D. Isheim, R. Kirchheim, F. Müller, and H. Kreye, Nanocrystalline Ni–3.6 at.% P and its transformation sequence studied by atom-probe field-ion microscopy, *Acta Mater.*, 48(2000), No. 4, p. 933.
[31] A. Farzaneh, M. Mohammadi, M. Ehteshamzadeh, and F. Mohammadi, Electrochemical and structural properties of electroless Ni–P–SiC nanocomposite coatings, *Appl. Surf. Sci.*, 276(2013), p. 697.
[32] J.Q. Gao, L. Liu, Y.T. Wu, B. Shen, and W.B. Hu, Electroless Ni–P–SiC composite coatings with superfine particles, *Surf. Coat. Technol.*, 200(2006), No. 20-21, p. 5836.
[33] C.K. Chen, H.M. Feng, H.C. Lin, and M.H. Hon, The effect of heat treatment on the microstructure of electroless Ni–P coatings containing SiC particles, *Thin Solid Films*, 416(2002), No. 1-2, p. 31.
[34] M. Franco, W. Sha, G. Aldic, S. Malinov, and H. Çimenoğlu, Effect of reinforcement and heat treatment on elevated temperature sliding of electroless Ni–P/SiC composite coatings, *Tribol. Int.*, 97(2016), p. 265.